Supporting Online Material For

A ROP GTPase signaling pathway controls microtubule ordering and cell expansion in *Arabidopsis*

Ying Fu[1,2¶], Tongda Xu[2], Lei Zhu[1], Mingzhang Wen[2], and Zhenbiao Yang[2¶]

[1]State Key Laboratory of Plant Physiology and Biochemistry, Department of Plant Sciences, College of Biological Sciences, China Agricultural University, Beijing 100193, China

[2]Center for Plant Cell Biology, Department of Botany and Plant Sciences, University of California, Riverside, CA 92521

[¶] To whom correspondence should be addressed.

E-mail: yingfu@cau.edu.cn, zhenbiao.yang@ucr.edu

Included:

Materials and Methods

Figure S1-S6

Reference

Materials and Methods

Plant Materials and Growth Conditions

Arabidopsis thaliana ecotypes Col-0 and WS were used in this study. Generation of *RIC1* overexpressing and knockout lines was as described [1]. The *α-tubulin-GFP* transgenic line was kindly provided by Dr. T. Hashimoto [2]. Plants were grown in soil or on Murashige and Skoog agar plates at 22ºC with 16-hr light/8-hr dark cycles, unless otherwise indicated.

Plasmid Construction

pBI221:GFP-mTalin and *pBI221:GFP-RIC1* were as described [1, 3]. For FRET experiments, GFP from the *pBI221:GFP-RIC1* was replaced with CFP. *ROP6* was amplified by PCR and cloned into the BglII and BamHI sites of *pBS35S:YFP* (kindly provided by Dr. A. von Arnim). *CA-rop6* (Q64L) and *DN-rop6* (D121A) were generated by use of the Quick Change Site-Directed Mutagenesis Kit (Qiagen, Valencia, CA) and cloned into BglII and BamHI sites of *pBS35S:YFP*.

Generation of Arabidopsis ROP6 Overexpressing and Knockout Lines

The *ROP6* T-DNA insertion mutant was screened from the K. Feldman collection available from the Ohio State University Arabidopsis Biological Resource Center (ABRC). PCR and DNA gel blot analyses were used to identify *ROP6* T-DNA insertion pools. For transgenic expression of GFP-ROP6, PCR-amplified *ROP6* was cloned into *pEGAD* vector (kindly provided by Dr. Chentao Lin) to generate GFP-tagged *ROP6* driven by the 35S promoter. The construct was introduced into *A. thaliana* ecotype Col-0 by *Agrobacterium*-mediated transformation [4]. The *ROP6* native promoter (2 kb

upstream of *ROP6* 5'UTR) was used to replace the 35S promoter in *pEGAD-ROP6* to generate *pROP6::GFP-ROP6*, which was introduced into the *rop6-1* knockout line for the complementation experiment.

Co-immunoprecipitation (co-IP) of GFP-ROP6 and RIC1

The interaction between native ROP6 and RIC1 was detected by a co-IP method that is designed specifically for transient or dynamic protein complex [5, 6]. Protoplasts were isolated from transgenic plants expressing GFP alone (as control) and those expressing GFP-ROP6. The protoplasts were homogenized in NEB buffer (20 mM HEPES [pH 7.5], 40mM KCl, 1mM EDTA, 1% Triton X-100, 1mM PMSF and protease inhibitor cocktail [Sigma]) using a ultrasonic device, and then centrifuged at 13000rpm for 15 mins at 4°C. Anti-GFP antibody conjugated with protein A-agarose beads (Santa cruz Cat No#sc-9996 ac) was incubated with protein extract supernatant in NEB buffer for 1 hr at 4°C on a rocker. The mixture was spinned at 3,000 rpm for 20 sec. After discarding the supernatant, beads were washed for five times (20 sec each wash) with the wash buffer (20 mM HEPES [pH 7.5], 40mM KCl, 1mM EDTA, 0.1% Triton X-100). The beads with the bound proteins were boiled in the 5×SDS-PAGE sample buffer, and analyzed by immunoblotting with purified anti-RIC1 antibody (1).

Ballistics-Mediated Transient Expression in Leaf Epidermal Cells

All plasmids were purified by using the QIAprep Mini prep kit (Qiagen; Valencia, CA). To observe the localization of GFP- or YFP-tagged protein, 0.8 μg constructs were used for bollistics-mediated transformation into leaf epidermal pavement cells as previously

described [3]. For FRET analysis, 1.0 μg *pBI221:CFP-RIC1* and 0.5 μg *pBS35S:YFP-ROP6/ pBS35S:YFP-DN-rop6* were co-transformed.

Confocal Microscopy

Confocal images were collected using a Leica TCS SP2 confocal microscope as described [1]. For visualizing leaf pavement cell or hypocotyl epidermis in the wild type and mutants, young leaves (usually the third true leaf from 2-week-old seedlings, unless otherwise indicated) or hypocotyls of 7-day-old seedlings were placed on a slide and imaged by confocal scanning using a UV laser. Auto fluorescence emitted from cells under excitation of UV clearly displayed the cell shape. For 3-D reconstruction, series of optical sections were taken at 0.5- to 1.0-μm increments (for sub-cellular localization with a 63x water lens) or 2 μm increments (for cell shape analysis with a 20x water lens) by use of Leica software. Additional image analysis and processing involved use of MetaMorph 4.5 and Adobe Photoshop 5.5. A cartoon in Fig.1D illustrates how the neck widths were measured. All the measurements were repeated using in a double blind fashion. For each line, 3 leaves or 3 cotyledons from 3 individual seedlings were scanned. The t-test is used for statistical analysis.

FRET Analysis

pBI221:CFP-RIC1 was transiently co-expressed with *pBS5S:YFP-rop6* and *pBS35S:YFP-DN-rop6*. FRET analysis was performed 4-7 hr after particle bombardment as described [1]. In brief, cells with strong or week fluorescence were excluded and those with medium expression levels were scanned and images were processed with a

MetaMorph software to measure the fluorescence intensity of the cell cortex (see Figure 3A for illustration of measured area. In brief, a region of interest (ROI) was drew around the fluorescent PM and cortex in the image collected from CFP channel, the ROI then was copied to YFP image as well as FRET image at exactly the same place using MetaMorph software. This ensured the measurements were done precisely within the same region). Due to non-FRET signals (CFP bleed-through to FRET channel and YFP excitation by 442-nm laser), correction factors were calculated from CFP donor alone and YFP acceptor alone controls. Factor <a> was calculated from YFP acceptor alone control: CFP channel emission of YFP acceptor (excited by 442-nm laser) divided by YFP channel emission of YFP acceptor (excited by 514 nm laser). Factor <b> was calculated from CFP donor alone control: YFP channel emission of CFP donor (excited by 442-nm laser) divided by CFP channel emission of CFP donor (excited by 442 nm laser). Factor <c> was also calculated from YFP acceptor alone control: YFP channel emission of YFP (excited by 442-nm laser) divided by YFP channel emission of YFP (excited by 514-nm laser).

For FRET analysis, following data were collected from cells co-expressing CFP donor and YFP acceptor:

Data <A>: CFP channel emission with 442-nm laser excitation

Data <B>: YFP channel emission with 442-nm laser excitation

Data <C>: YFP channel emission with 514-nm laser excitation

Corrected FRET signal = B-b*A-(c-a*b)*C

To exclude the interference of cell to cell variability in transient expression levels, corrected FRET signal was normalized with the acceptor amount for comparison, which

is FRET efficiency, % of YFP emission that results from FRET (i.e., corrected FRET signal divided by YFP emission excited by 514-nm laser).

RIC1 and Microtubule Immunolocalization

Mouse anti-α-tubulin antibody (1:300, Sigma) and TRITC-conjugated anti-mouse IgG (1:200, Sigma) were used for MT staining; Rabbit anti-RIC1 antibody (1:200) [1] and FITC-conjugated anti-rabbit IgG (1:200) were used for RIC1 staining; the immunostaining protocol was as described [7] with modified fixation methods: detached leave were submerged by the fixative (50mM PIPES, 5nM EGTA, 1mM $MgCl_2$, 4% paraformaldehyde, 0.1% glutaraldehyde and 0.05% Triton X-100) right away and cut into 2x2 mm pieces, then they were transferred in to small vials and gently vacuumed for better infiltration. The samples were analyzed by use of the Leica TCS SP2 confocal microscope system.

Supplementary Figure Legends

Figure S1. Quantitative analysis of *rop6-1* and *ric1-1* cell shape phenotypes in double blind fashion.

(A) Quantitative analysis of pavement cell neck widths for WS, *rop6-1, ric1-1, and rop6-1;ric1-1* double mutants conducted blindly. In consistent with Figure 1D, the differences in neck widths between WS and other mutants or double mutant line were significant ($p<0.05$, t-test), with no significant differences between the *rop6-1;ric1-1* double mutant and *rop6-1* or *ric1-1* single mutant. In each line, a total of

about 300 cells from 3 seedlings was measured. All data are means ± standard deviation.

(B) Quantitative analysis of hypocotyl cell widths in wild type (WT), *ric1-1* and *rop6-1* lines conducted blindly. In consistent with Figure 4B, there was significant differences in widths between WT and *ric1-1* or *rop6-1* ($P<0.05$, t-test). The mean width of *rop6-1* cells appeared slightly narrower than that of *ric1-1* cells, but the difference was not significant ($p>0.05$, t-test). In each line, a total of more than 300 cells from 3 seedlings was measured. All data are means ± standard deviation.

Figure S2: Expression of *GFP-ROP6* suppressed *rop6-1* cell-shape phenotype.

pROP6:GFP-ROP6 was transformed into the *rop6-1* line. T1 lines resistant to BASTA were chosen for transcript level and phenotypic analysis. Two lines with levels of transgenic *GFP-ROP6* expression equivalent to the level of wild type *ROP6* were chosen for analysis.

(A) RT-PCR analysis of *ROP6* transcript levels in wild type (WT) and *pROP6::GFP-ROP6* transformed lines.

(B) Quantitative analysis of widths of cell necks between two nearest opposing indenting regions. Shown is *rop6-1* pavement-cell phenotype fully recovered by expressing GFP-ROP6 at a similar level as native ROP6 in the wild type. There is no significant difference between WT and two complemented lines ($p\geq0.05$, t-test). All data are means ± standard deviation.

Figure S3: Phenotype analysis of different ROP6-overexpressing lines.

(A) Cotyledon epidermal cells display various phenotypes in different ROP6-overexpressing lines (*ROP6-1*, *ROP6-3* and *ROP6-5*). Severe phenotypes (narrower indenting neck and rare lobes) were found in lines *ROP6-1* and *ROP6-3*, with dramatically higher *ROP6* transcript levels than those of the *ROP6-5* line and the WT. *ROP6-5* is a weaker line with *ROP6* transcript level somewhat higher than that of the WT, and accordingly with the mean cell width and lobe length significantly lower than those of the wild type.

(B) RT-PCR analysis of *ROP6* transcript levels in wild type (WT) and different *ROP6* overexpressing lines.

(C) Quantitative analysis of the mean width of indenting neck regions. The difference between the WT and *ROP6-5* is significant ($p<0.05$, t-test). All data are means ± standard deviation.

(D) Quantitative analysis of mean length of lobes. The difference between WT and *ROP6-5* is significant ($p<0.05$, t-test). All data are means ± standard deviation.

Figure S4. ROP6 inhibited the fine microfilament (MF) formation.

MF localization in wild type and different *RIC1* and *ROP6* mutant backgrounds was visualized by use of GFP-mTalin (actin-binding domain). GFP-mTalin was transiently expressed in the pavement cells of indicated lines as described [1, 3]. Fine MFs (arrowheads) were associated with lobes in wild-type cells. Absence of ROP6 or RIC1 caused over-accumulation of cortical fine F-actin throughout most part of the cell cortex. In contrast, overexpression of ROP6 or RIC1 reduced the fine cortical MF population, leading to thicker F-actin cables (arrows). This population of fine MFs was greatly

reduced in 87% (n=31) of the ROP6-overexpressing cells (*ROP6 OX-3* stage I and II cells) but increased in 81% (n=47) of *rop6-1* cells (stage I and II)

Figure S5. ROP6 is required for RIC1 association with cortical MTs.

(A) Anti-RIC1 immunostaining showed RIC1 localization as a dotted-line pattern in WT cells as described previously [1]. In rop6-1 cells, however, RIC1 staining was found in certain regions of the cell cortex, particularly enriched in lobing regions, and rarely found in a dotted line pattern.

(B) Co-immunolocalization of RIC1 and cortical MTs in wild type (WT) and *rop6-1* mutant cells. Pavement cells were co-stained with anti-RIC1 and anti-tubulin antibodies. In WT cells, RIC1 was localized as punctuates along cortical MTs, especially rich in indentation region, where thick transverse MT cables located (arrows). However, in *rop6-1* cells, RIC1 was not associated with MTs but was enriched in lobe tip regions.

References

1. Fu, Y., Gu, Y., Zheng, Z., Wasteneys, G., and Yang, Z. (2005). Arabidopsis interdigitating cell growth requires two antagonistic pathways with opposing action on cell morphogenesis. Cell *120*, 687-700.
2. Ueda, K., Matsuyama, T., and Hashimoto, T. (1999). Visualization of microtubules in living cells of transgenic Arabidopsis thaliana. Protoplasma *206*, 201-206.
3. Fu, Y., Li, H., and Yang, Z. (2002). The ROP2 GTPase controls the formation of cortical fine F-actin and the early phase of directional cell expansion during Arabidopsis organogenesis. Plant Cell *14*, 777-794.

4. Clough, S.J., and Bent, A.F. (1998). Floral dip: a simplified method for Agrobacterium-mediated transformation of Arabidopsis thaliana. Plant J *16*, 735-743.
5. Gampala, S.S., Kim, T.-W., He, J.-X., Tang, W., Deng, Z., Bai, M.-Y., Guan, S., Lalonde, S., Sun, Y., Gendron, J.M., et al. (2007). An Essential Role for 14-3-3 Proteins in Brassinosteroid Signal Transduction in Arabidopsis. *13*, 177-189.
6. Liu, H., Yu, X., Li, K., Klejnot, J., Yang, H., Lisiero, D., and Lin, C. (2008). Photoexcited CRY2 Interacts with CIB1 to Regulate Transcription and Floral Initiation in Arabidopsis. science *322*, 1535-1539.
7. Wasteneys, G.O., Willingale-Theune, J., and Menzel, D. (1997). Freeze shattering: a simple and effective method for permeabilizing higher plant cell walls. J Microsc *188*, 51-61.

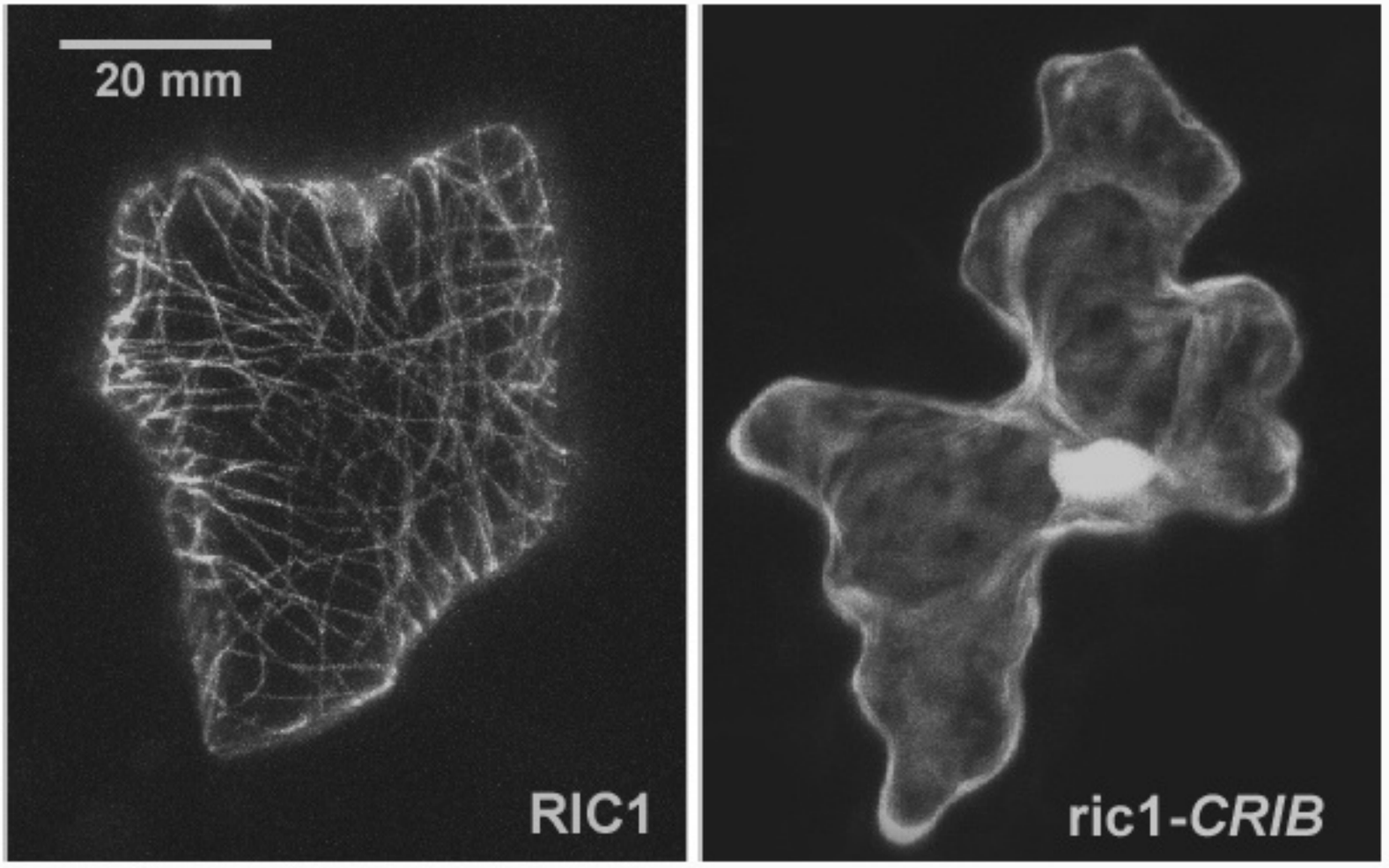

Fig. S1

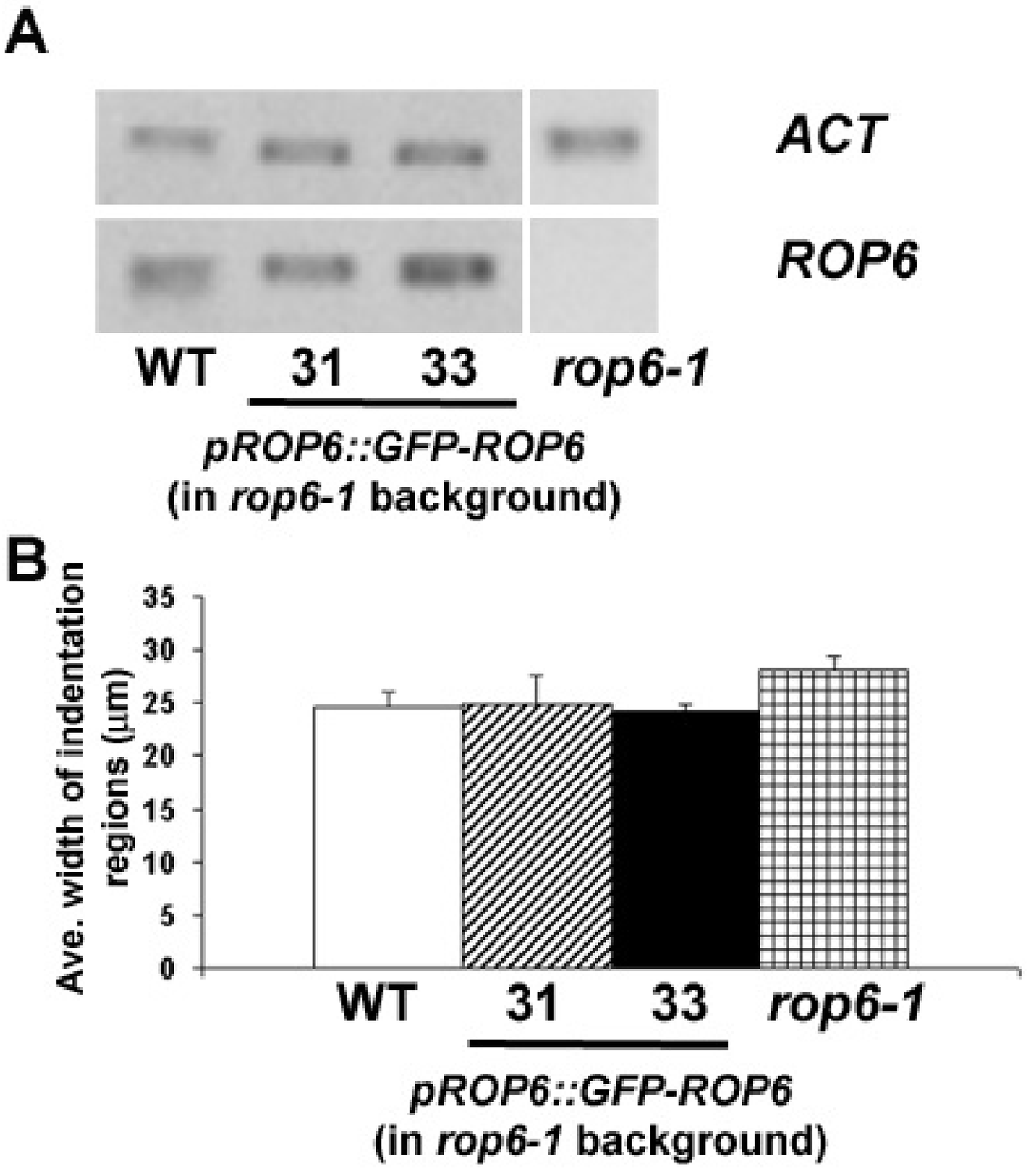
A
ACT
ROP6
WT
31
33
rop6-1
pROP6::GFP-ROP6
(in rop6-1 background)
B
Ave. width of indentation regions (μm)
35
30
25
20
15
10
5
0
WT
31
33
rop6-1
pROP6::GFP-ROP6
(in rop6-1 background)

Fig. S2

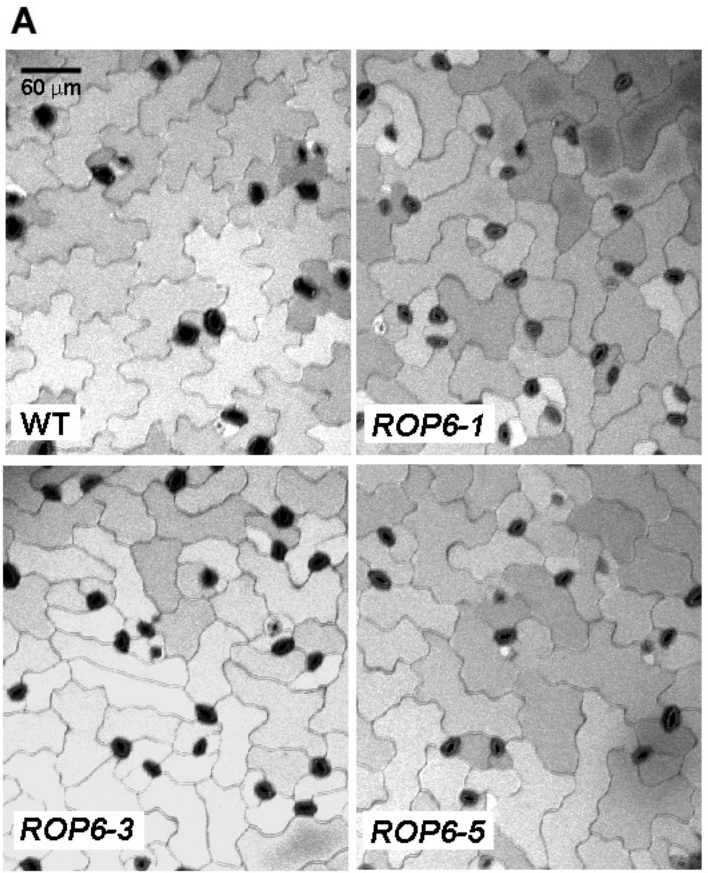
A
60 μm
WT
ROP6-1
ROP6-3
ROP6-5
B
ACT
ROP6
WT
1
3
5
ROP6OE
C
Ave. width of neck regions (μm)
40
35
30
25
20
15
10
5
0
WT
ROP6-5
D
Ave. length of lobes (μm)
20
18
16
14
12
10
8
6
4
2
0
WT
ROP6-5

Fig. S3

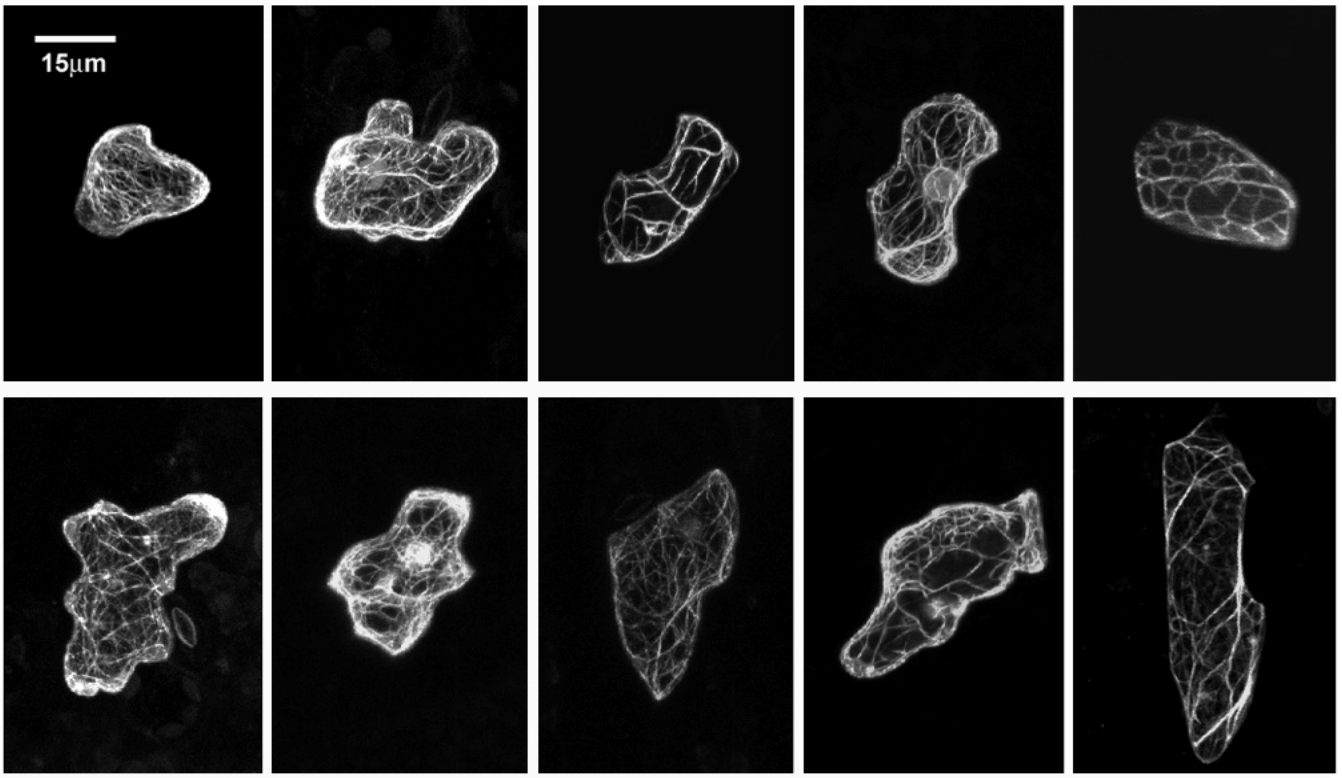

Fig. S4

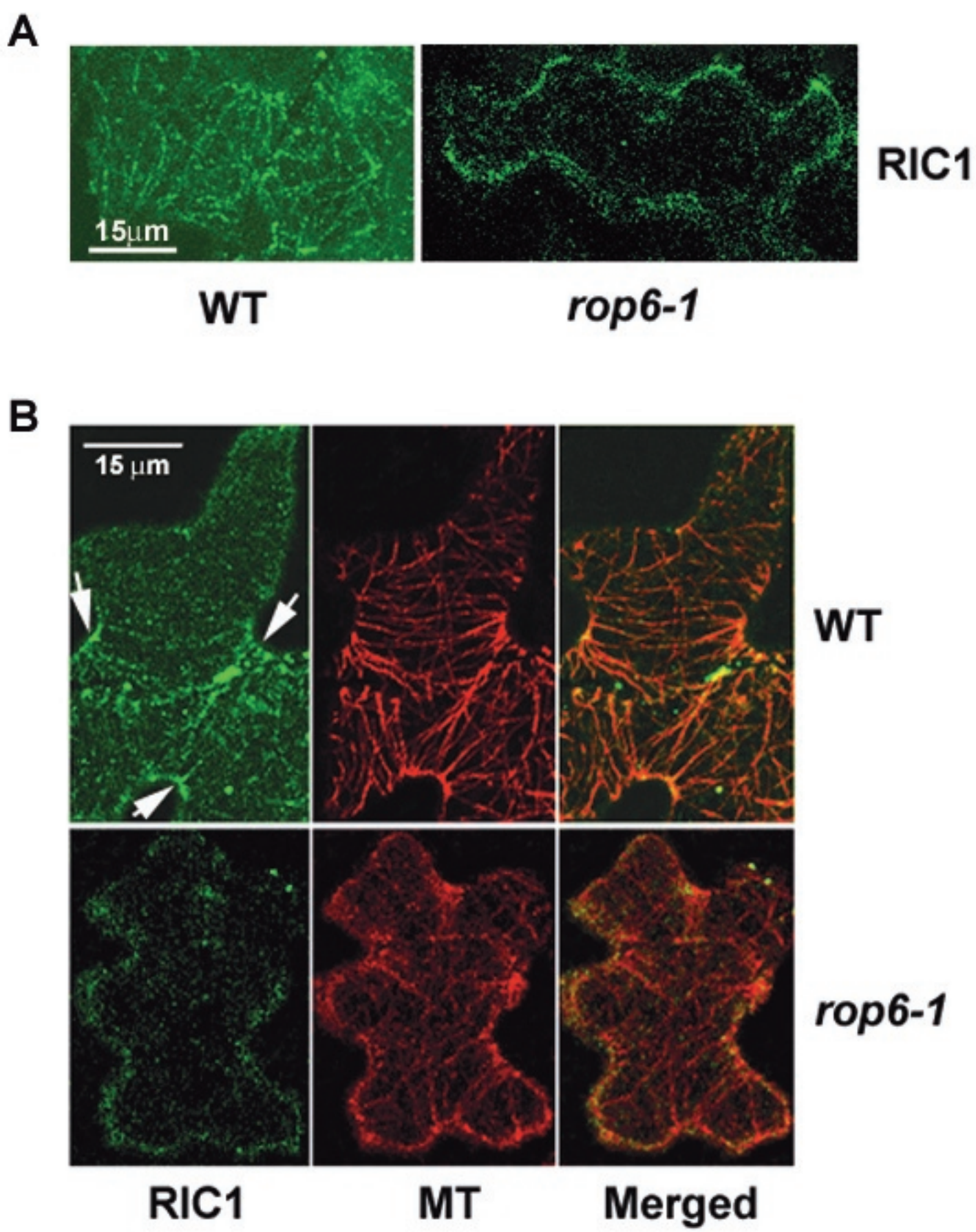

Fig. S5